

Offline Identification of Induction Machine Parameters With Core Loss Estimation Using the Stator Current Locus

David M. Reed, *Member, IEEE*, Heath F. Hofmann, *Senior Member, IEEE*, and Jing Sun, *Fellow, IEEE*

Abstract—High-performance control of induction machines in electric drives requires accurate knowledge of the machine parameters. While parameters have traditionally been identified using the standard no-load and locked-rotor tests, performing the locked-rotor test as prescribed in the IEEE standard requires special test equipment, and is difficult to implement with an inverter due to the low voltages involved. This paper presents a new method for induction machine parameter identification, including core loss conductance, which is based on fitting steady-state experimental data to the stator current locus for various slip frequencies in the stator flux linkage reference-frame. Numerical analysis confirms the accuracy of the method, while experimental results demonstrate its ability to characterize an induction machine over a range of flux levels which include magnetic saturation. Finally, it is shown that model-based predictions of the steady-state machine behavior computed using the parameter estimates provided by the proposed technique are more accurate than those obtained using the IEEE standard, when compared to measurements of the power factor, three-phase input power, and RMS line current.

Index Terms—Induction machine, stator current locus, parameter identification, core loss estimation.

I. INTRODUCTION

HISTORICALLY, induction machines have been the industrial workhorse while permanent magnet machines have dominated high-performance applications. However, advancements in their design and control have made induction machines a viable alternative to permanent magnet machines in automotive applications (e.g., the Tesla Model S) where ruggedness and the absence of expensive rare-earth magnets are desirable characteristics. Nevertheless, the challenge remains that high-performance control techniques, such as field-oriented control, require accurate knowledge of the machine parameters [1].

Over the past few decades, a considerable amount of attention has been given to the online identification of the rotor time constant and/or rotor resistance, e.g., [2]–[7], as these parameters

can vary significantly with temperature, leading to severe detuning in both direct and indirect field-oriented controllers [1], [8]. In addition to the rotor time constant, online techniques have been proposed for other machine parameters as well, e.g., [9]–[12]. However, the added complexity and design difficulty of adaptive parameter estimation might not be appropriate for some applications. Furthermore, since the variations in some machine parameters, such as inductance, may be modeled as functions of known or measurable variables such as flux linkage magnitude and temperature, offline identification of such machine parameters for non-adaptive control methodologies is a viable alternative.

The IEEE standard for induction machine parameter identification [13] uses no-load and locked-rotor tests for offline parameter identification. However, accurate parameter estimation using the standard requires special equipment to conduct these tests. For example, it is recommended that locked-rotor tests be conducted at electrical frequencies close to typical slip frequencies (e.g., 25% of rated frequency) to obtain accurate leakage inductance and rotor resistance estimates. While a voltage-source inverter could be used to generate the necessary variable frequency voltage waveforms, the presence of switching harmonics in the output voltage necessitates the addition of an LC-filter to remove switching harmonics, ensuring that limitations on total harmonic distortion are not violated. Additionally, for high-speed machine designs, the reduced frequency (25% of rated) recommended by the IEEE standard for the locked-rotor test may still be too high, leading to larger estimates of the rotor resistance.

Alternatives to the IEEE standard for offline identification of induction machine parameters have been proposed, which can generally be categorized as using either transient measurements (e.g., [14]–[19]) for parameter identification, or steady-state measurements (e.g., [20]–[25]), like the technique proposed in this paper. In one reference [20], an adaptive (search boundary) genetic algorithm is used to identify machine parameters, while a more recent paper [21] has proposed using the Levenberg-Marquardt algorithm, commonly used to solve nonlinear least-squares problems, to estimate induction machine parameters. Other approaches have been proposed as well [22], [23] which use variable frequency tests at a standstill (i.e., zero rotor speed) to estimate parameters. However, with the exception of [24], [25], none of these papers [14]–[23] considers core loss in their parameter identification, which can influence the accuracy of estimated parameters [26], [27]. Nor is the characterization of magnetic saturation considered beyond noting that

Manuscript received November 25, 2015; revised May 7, 2016; accepted August 10, 2016. Date of publication August 18, 2016; date of current version November 22, 2016. This work was supported by the U.S. Office of Naval Research under Grant 00014-11-1-0831. Paper no. TEC-00868-2015.

D. M. Reed is with the Department of Aerospace Engineering, University of Michigan, Ann Arbor, MI 48109 USA (e-mail: davereed@umich.edu).

H. F. Hofmann is with the Department of Electrical Engineering and Computer Science, University of Michigan, Ann Arbor, MI 48109 USA (e-mail: hofmann@umich.edu).

J. Sun is with the Department of Naval Architecture and Marine Engineering, University of Michigan, Ann Arbor, MI 48109 USA (e-mail: jingsun@umich.edu).

Color versions of one or more of the figures in this paper are available online at <http://ieeexplore.ieee.org>.

Digital Object Identifier 10.1109/TEC.2016.2601781

it can have an influence on the estimated parameters [16]–[19], [22], [23].

This paper presents a new technique for induction machine parameter identification using steady-state current measurements, which is well suited to modern VSI drive systems and avoids the difficulties associated with inverter-based implementations of the locked-rotor test. The proposed technique is based on fitting experimental data to the circular stator current locus in the stator flux linkage reference-frame for varying steady-state slip frequencies, and provides a decoupling between the identification of the magnetic parameters and the identification of the rotor resistance. This decoupling is due to the fact that the radius and center location of the circular current locus are determined by the magnetic parameters and core loss conductance, independent of the rotor resistance and its variations. Thus, by fitting a circle to experimental data, accurate estimates of the magnetic parameters, as well as the core loss conductance, are obtained. The rotor resistance is then estimated by performing a least-squares fit of the experimental data to a steady-state induction machine model. Numerical simulation results evaluating the accuracy of the estimated parameters in the presence of non-ideal effects are presented, and experimental results for a 43 kW induction machine are provided which demonstrate the utility of the proposed technique by characterizing the machine over a wide range of flux levels (i.e., stator flux linkage magnitudes), including magnetic saturation. Additionally, it is shown that model-based predictions of the steady-state machine behavior computed using the parameter estimates provided by the proposed technique are more accurate than those obtained using the IEEE standard, when compared to measured values. Finally, this paper represents a significant extension of our conference paper on the topic [28]. Specifically, we have:

- 1) extended the technique to include core loss conductance in the model and estimation;
- 2) improved the stator flux linkage estimators by incorporating nulling of DC offset measurement errors;
- 3) provided extensive simulation results capturing many of the non-ideal effects encountered in practice; and
- 4) included a detailed mathematical derivation of the stator current locus.

II. THE STEADY-STATE STATOR CURRENT LOCUS

In this work, the induction machine is modeled as having a smooth air-gap (i.e., slotting effects are neglected) in addition to the following simplifying assumptions:

- A1.** a quasi-linear magnetics model;
- A2.** the machine is balanced in its construction with sinusoidally-distributed magnetomotive force (mmf);
- A3.** a 1:1 effective turns ratio;
- A4.** the core loss is modeled as a resistive shunt just after the stator winding resistance (see Fig. 1).

The first assumption, **A1**, permits variations in the magnetic parameters with operating conditions, while **A2** justifies the use of a 2-phase equivalent model and transformation from 3-phase to 2-phase using the Clarke transform [29]. The third

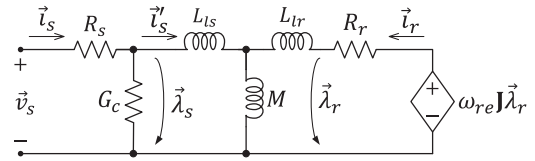


Fig. 1. Dynamic 2-phase equivalent circuit model for an induction machine.

assumption, **A3**, is common for squirrel-cage induction machines. Finally, while core loss is typically modeled as a resistance in parallel with the mutual inductance, this placement is somewhat arbitrary as leakage flux also travels through the machine iron. **A4** simplifies the analysis while still capturing the nature of the core loss (i.e., electrical power which is not converted into mechanical power).

The desired expressions for the steady-state stator currents in the stator flux linkage reference-frame are developed starting from the flux linkage dynamics in the stationary reference-frame for the 2-phase equivalent induction machine model:

$$\frac{d\vec{\lambda}_s}{dt} = -R_s \vec{i}_s + \vec{v}_s, \quad (1)$$

$$\frac{d\vec{\lambda}_r}{dt} = -R_r \vec{i}_r + \omega_{re} \mathbf{J} \vec{\lambda}_r, \quad (2)$$

where $\vec{\lambda}_s = [\lambda_{sd} \ \lambda_{sq}]^T$ is the stator flux linkage vector, $\vec{\lambda}_r = [\lambda_{rd} \ \lambda_{rq}]^T$ is the rotor flux linkage vector, $\vec{i}_s = [i_{sd} \ i_{sq}]^T$ is the stator current vector, $\vec{i}_r = [i_{rd} \ i_{rq}]^T$ is the rotor current vector, $\vec{v}_s = [v_{sd} \ v_{sq}]^T$ is the stator voltage vector, and \mathbf{J} is the 90° CCW rotation matrix. These expressions (1) and (2) are easily derived by applying Kirchhoff's laws to the equivalent circuit model provided in Fig. 1.

To represent (2) in the stator flux linkage reference-frame, we use the Park transform [30],

$$\vec{x}^{\lambda_s} = e^{-\mathbf{J}\theta_{\lambda_s}} \vec{x}, \quad (3)$$

where the superscript λ_s is used to designate variables which are being represented in the the stator flux linkage reference-frame, the angle of which is denoted by θ_{λ_s} . Applying (3) to the stationary-frame electrical variables in (2) yields

$$\frac{d\vec{\lambda}_r^{\lambda_s}}{dt} = -R_r \vec{i}_r^{\lambda_s} + \omega_{se} \mathbf{J} \vec{\lambda}_r^{\lambda_s}, \quad (4)$$

where $\omega_{se} = \omega_e - \omega_{re}$ is the electrical slip frequency. At steady-state¹ (4) gives us the following expression for the steady-state rotor currents

$$\vec{I}_r^{\lambda_s} = -\frac{\Omega_{se}}{R_r} \mathbf{J} \vec{\Lambda}_r^{\lambda_s}, \quad (5)$$

where Ω_{se} is the steady-state electrical slip frequency. Using the fact that²

$$\vec{\lambda}_r^x = \frac{\sigma^2}{L_s} \vec{i}_r^x + \frac{M}{L_s} \vec{\lambda}_s^x, \quad (6)$$

¹Steady-state variables are denoted by capital letters.

²The following flux linkage/current relationships hold for arbitrary reference-frames, x , and may be used to derive equations (6) and (10): $\vec{\lambda}_s^x = L_s \vec{i}_s^x + M \vec{i}_r^x$ and $\vec{\lambda}_r^x = M \vec{i}_s^x + L_r \vec{i}_r^x$, where $L_s = L_{1s} + M$ and $L_r = L_{1r} + M$.

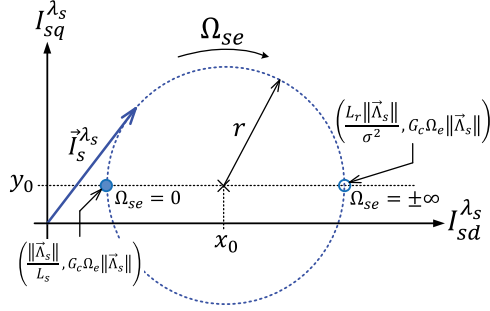


Fig. 2. Parameterized steady-state stator current locus in the stator flux linkage reference-frame.

where $\sigma^2 = L_s L_r - M^2$, we obtain the following expression for the steady-state rotor currents in the stator flux linkage reference-frame as a function of slip frequency and stator flux linkage

$$\vec{I}_r^{\lambda_s} = -\frac{\Omega_{se} \frac{M}{R_r L_s}}{1 + \left(\frac{\Omega_{se} \sigma^2}{R_r L_s}\right)^2} \left[\frac{\Omega_{se} \sigma^2}{R_r L_s} \mathbf{I} + \mathbf{J} \right] \vec{\Lambda}_s^{\lambda_s}, \quad (7)$$

where \mathbf{I} is the identity matrix.

Finally, using the stator current relationship with core loss (as defined in Fig. 1),

$$\vec{i}_s = G_c \frac{d\vec{\lambda}_s}{dt} + \vec{i}_s', \quad (8)$$

which, at steady-state and when represented in the stator flux linkage reference-frame, is given by

$$\vec{I}_s^{\lambda_s} = G_c \Omega_e \mathbf{J} \vec{\Lambda}_s^{\lambda_s} + \vec{I}_s'^{\lambda_s}, \quad (9)$$

along with the fact that

$$\vec{I}_s'^{\lambda_s} = \frac{1}{L_s} \left(\vec{\Lambda}_s^{\lambda_s} - M \vec{I}_r^{\lambda_s} \right), \quad (10)$$

we obtain the desired scalar form expressions for the steady-state stator currents represented in the stator flux linkage reference-frame in which the direct-axis is aligned with the stator flux linkage vector (i.e., $\vec{\lambda}_s^{\lambda_s} = [||\vec{\lambda}_s|| \ 0]^T$):

$$I_{sd}^{\lambda_s} = \left[1 + \left(\frac{M}{\sigma}\right)^2 \frac{(\Omega_{se}/\Omega_{se,\max}^{\lambda_s})^2}{1 + (\Omega_{se}/\Omega_{se,\max}^{\lambda_s})^2} \right] \frac{||\vec{\Lambda}_s||}{L_s}, \quad (11)$$

$$I_{sq}^{\lambda_s} = \left(\frac{M}{\sigma}\right)^2 \frac{(\Omega_{se}/\Omega_{se,\max}^{\lambda_s})}{1 + (\Omega_{se}/\Omega_{se,\max}^{\lambda_s})^2} \frac{||\vec{\Lambda}_s||}{L_s} + G_c \Omega_e ||\vec{\Lambda}_s||, \quad (12)$$

where Ω_e is the steady-state electrical frequency, $||\vec{\Lambda}_s||$ is the stator flux linkage magnitude and $\Omega_{se,\max}^{\lambda_s} = \frac{R_r L_s}{\sigma^2}$ is the slip frequency which maximizes torque for a given stator flux linkage magnitude.

When plotted as a function of slip frequency, (11) and (12) produce the circular stator current locus in Fig. 2. The parameterized stator current locus circle is given by

$$\left(I_{sd}^{\lambda_s} - x_0\right)^2 + \left(I_{sq}^{\lambda_s} - y_0\right)^2 = r^2, \quad (13)$$

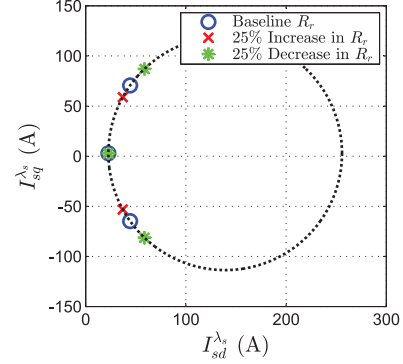


Fig. 3. Numerical analysis demonstrating the influence of a 25% increase in the rotor resistance, R_r , on the stator current locus.

where,

$$x_0 = \frac{1}{2} \left(\frac{1}{L_s} + \frac{L_r}{\sigma^2} \right) ||\vec{\Lambda}_s||, \quad (14)$$

$$y_0 = G_c \Omega_e ||\vec{\Lambda}_s||, \quad (15)$$

$$r = \frac{M^2}{2\sigma^2 L_s} ||\vec{\Lambda}_s||. \quad (16)$$

The stator current locus in Fig. 2 can therefore be used to identify the magnetic parameters of the induction machine, as well as the core loss conductance, by fitting the parametric circle (13) to experimental data which forms the stator current locus, provided that the stator flux linkage magnitude is held constant (i.e., regulated) during data collection. Additionally, note that neither the center location (14) and (15), nor the radius (16), depend on the rotor resistance, R_r . This is demonstrated numerically in Fig. 3. Using (11) and (12) we compute the direct and quadrature axis stator currents for various slip frequencies with nominal and increased rotor resistance. As demonstrated in Fig. 3, changes in the rotor resistance will cause the locus points to either “stretch” or “shrink” *along* the locus circle without affecting either the radius or center location.

Once estimates of the center location, (\hat{x}_o, \hat{y}_o) , and radius, \hat{r} , have been computed, the core loss and magnetic parameters are calculated assuming that the inductance ratio, $\frac{L_s}{L_r}$, is known.³ This assumption gives us three equations with three unknowns, $L_{s,r}$, M , and G_c . Once we have estimates of the magnetic parameters and the core loss conductance, (11) and (12) along with the corresponding slip frequencies, are used to estimate the rotor resistance. Since the magnetic parameters are obtained from the parameterization of the fitted locus circle (14)–(16), their estimates are independent of the rotor resistance, which can vary significantly due to ohmic heating during data collection. Other benefits of the proposed technique are a reduction in the dimension of the estimation problem by identifying magnetic parameters (and core loss conductance) independently from the rotor resistance, the use of multiple measurement points in estimating parameters, and the ability to characterize the machine

³If the NEMA-design letter is known, this ratio can be found in IEEE Standard 112; otherwise assume $L_s/L_r = 1$.

over a wide range of operating points which include magnetic saturation.

III. PROPOSED PARAMETER ESTIMATION TECHNIQUE

A. Fitting the Parameterized Stator Current Locus Circle to Data

Using the stator current locus presented in the previous section, the magnetic parameters, as well as the core loss conductance, are identified by fitting the parameterized circle (Fig. 2) to experimental data. The fitting is achieved by solving a reasonably simple minimization problem. According to the theory, the zero-slip datum point and the center of the SCL should be aligned horizontally. While it may seem simplistic to use the zero-slip datum point to fix the center of the estimate stator current locus (circle), it works well in practice, as will be demonstrated in our numerical analysis.

Enforcing the condition that the zero-slip datum point determines the vertical offset in the locus circle, we see that

$$\hat{y}_o = I_{sq}(\Omega_{se} = 0). \quad (17)$$

The magnetic parameters are then computed by solving the following minimization problem

$$(\hat{x}_o, \hat{r}) = \arg \min_{(x,r)>0} J_{scl}(x, r), \quad (18)$$

where the cost function, $J_{scl}(x, r)$, is given by,

$$J_{scl} = \sum_{n=1}^N \left[r^2 - \left((I_{sd,n}^{\lambda_s} - x)^2 + (I_{sq,n}^{\lambda_s} - \hat{y}_o)^2 \right) \right]^2, \quad (19)$$

where $I_{sd,n}^{\lambda_s}$ and $I_{sq,n}^{\lambda_s}$ are the n^{th} measurements of the steady-state direct and quadrature stator currents in the stator flux linkage reference-frame. This approach (18) and (19) is sometimes referred to as a ‘‘pure least-squares’’ solution [31]. In our work, we chose to solve this minimization problem numerically using MATLAB’s *fmincon* constrained nonlinear programming algorithm.

Given estimates of the center location, (\hat{x}_o, \hat{y}_o) , and radius, \hat{r} , the stator self-inductance is given by

$$\hat{L}_s = \frac{\|\vec{\Lambda}_s\|}{\hat{x}_o - \hat{r}}. \quad (20)$$

Next, we assume that the stator and rotor inductances are the same (i.e. $\hat{L}_s/\hat{L}_r = 1$) and compute the leakage term:

$$\hat{\sigma}^2 = \frac{\hat{L}_r \hat{L}_s \|\vec{\Lambda}_s\|}{2 \hat{L}_s \hat{x}_o - \|\vec{\Lambda}_s\|}. \quad (21)$$

Once the self-inductance and leakage terms are known, the mutual inductance is calculated:

$$\hat{M} = \sqrt{\hat{L}_s \hat{L}_r - \hat{\sigma}^2}. \quad (22)$$

Finally, the estimate of the core loss conductance is given by

$$\hat{G}_c = \frac{\hat{y}_o}{\Omega_c \|\vec{\Lambda}_s\|}. \quad (23)$$

To estimate the rotor resistance, we will minimize the sum-of-squares error between the experimental datum points and those predicted by the steady-state model of the stator current locus (in the stator flux linkage reference-frame). Again, the parameter estimation is obtained by solving a constrained minimization problem where

$$\hat{R}_r = \arg \min_{R_r \in [R_r, \min, R_r, \text{MAX}]} J_{R_r}(R_r) \quad (24)$$

where the cost function, $J_{R_r}(R_r)$, is given by,

$$J_{R_r}(R_r) = \sum_{n=1}^N \left(\left(\hat{I}_{sd,n}^{\lambda_s} - \hat{I}_{sd,n}^{\lambda_s} \right)^2 + \left(\hat{I}_{sq,n}^{\lambda_s} - \hat{I}_{sq,n}^{\lambda_s} \right)^2 \right), \quad (25)$$

where $\hat{I}_{sd,n}^{\lambda_s}$ and $\hat{I}_{sq,n}^{\lambda_s}$ are functions of R_r given by:

$$\hat{I}_{sd,n}^{\lambda_s} = \left[1 + \frac{\hat{M}^2}{\hat{\sigma}^2} \frac{(\hat{\sigma}^2 \Omega_{se,n})^2}{(R_r \hat{L}_s)^2 + (\hat{\sigma}^2 \Omega_{se,n})^2} \right] \frac{\|\vec{\Lambda}_s\|}{\hat{L}_s}, \quad (26)$$

$$\hat{I}_{sq,n}^{\lambda_s} = \frac{\hat{M}^2}{\hat{\sigma}^2} \frac{R_r \hat{L}_s \hat{\sigma}^2 \Omega_{se,n}}{(R_r \hat{L}_s)^2 + (\hat{\sigma}^2 \Omega_{se,n})^2} \frac{\|\vec{\Lambda}_s\|}{\hat{L}_s} + \hat{G}_c \Omega_{e,n} \|\vec{\Lambda}_s\|. \quad (27)$$

Note that a non-zero stator flux linkage magnitude and non-zero slips are required for identification of the rotor resistance. This amounts to a rather intuitive persistent excitation condition [6] in that it suggests rotor currents must be present in order to determine the rotor resistance. While this cost function (25)–(27) is globally non-convex, it is convex for practical rotor resistance values (e.g., positive values) with a unique minimum at the true resistance. Therefore, we enforce constraints when solving the minimization problem, requiring that $R_r \in [0.1R_s, 10R_s]$. Once again, we use MATLAB’s *fmincon* constrained nonlinear programming algorithm to solve the minimization problem.

B. Procedure for Data Collection

In order to generate the experimental stator current locus, the measured stator currents must be projected into the stator flux linkage reference-frame using the Park transform (3). Additionally, the stator flux linkage magnitude must be held constant while the steady-state direct and quadrature stator currents are recorded for various steady-state (i.e., constant) slip frequencies, Ω_{se} . To ensure that the flux linkage magnitude remains constant, a Proportional-Integral (PI) regulator is used to drive the error between the commanded stator flux magnitude, $\|\vec{\Lambda}_s\|$, and estimated flux magnitude, $\|\hat{\Lambda}_s\|$, to zero. The output of the PI regulator is the stator excitation voltage magnitude, $\|\vec{v}_s\|$, as depicted in Fig. 4, and the generated direct and quadrature-axis voltage are given by,

$$\begin{aligned} v_{sd} &= \|\vec{v}_s\| \cos(\omega_e t), \\ v_{sq} &= \|\vec{v}_s\| \sin(\omega_e t). \end{aligned} \quad (28)$$

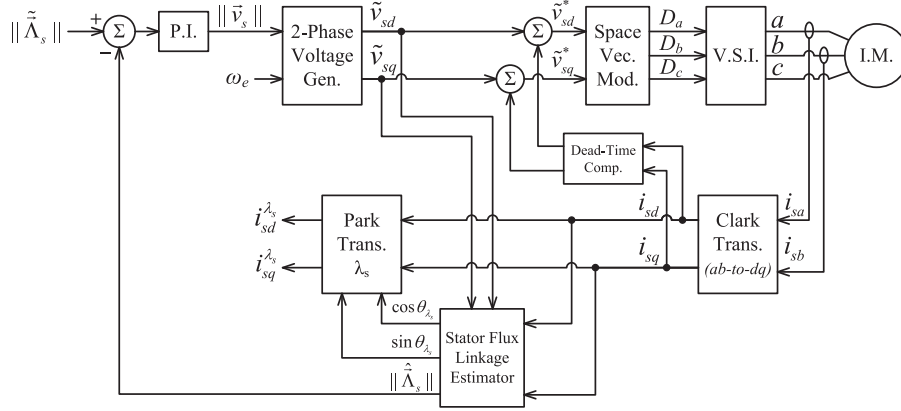


Fig. 4. Data acquisition controller block diagram for the proposed parameter estimation technique.

Finally, the slip frequency is varied by either fixing the electrical frequency, ω_e , of the stator excitation voltage and varying the regulated rotor speed of the load machine, or vice versa.

Selection of the electrical excitation frequency, ω_e , is somewhat arbitrary. In general, running at higher speeds (and thus, higher electrical frequencies) will reduce the influence of stator resistance variations, as well as inverter non-ideal effects like dead-time, by increasing voltage levels in the machine. Additionally, the electrical frequency should be high enough that the effects of integrator approximations are negligible. Similar to electrical frequency, the use of higher stator flux linkage magnitudes will also help to minimize the influence of stator resistance variations and inverter non-ideal effects (e.g., dead-time). However, it is advisable to consider multiple flux linkage magnitudes during data collection, to check at what point the machine (iron) begins to saturate. The nominal (or rated) specifications from the manufacturer are a good starting point for selecting the electrical frequency and stator flux linkage magnitude.

C. Dead-Time Compensation

In practical implementations, it is desirable to avoid the use of stator voltage measurements due to the added cost and complexity involved in processing the pulse-width modulated (PWM) voltage waveforms. Instead of measured voltages, our algorithm (Fig. 4) uses the commanded stator voltages to estimate the stator flux linkage. However, use of the commanded voltages requires compensation of non-ideal inverter characteristics such as the dead-time effect [8], which lead to distortions in the stator current locus, as depicted in Fig. 5. For this reason, first-harmonic dead-time compensation is employed to ensure that the actual voltages applied to the machine terminals closely resemble the commanded values used to estimate the stator flux linkage. In discrete-time and in the stationary reference-frame, the compensated voltage command, $\tilde{v}_{s,k}^* = [\tilde{v}_{sd,k}^* \ \tilde{v}_{sq,k}^*]^\top$, at time-step “ k ” is given by:

$$\tilde{v}_{s,k}^* = \tilde{v}_{s,k} + \frac{4}{\pi} V_{\text{bus}} t_d f_{\text{sw}} \left(e^{\mathbf{J}(1.5T_s \Omega_e)} \frac{\tilde{i}_{s,k}}{\|\tilde{i}_{s,k}\|} \right). \quad (29)$$

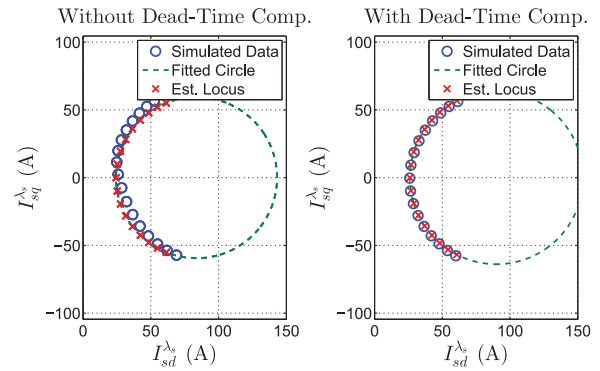


Fig. 5. Simulation results depicting distortion due to dead-time effect and improvement using first-harmonic dead-time compensation.

where $\tilde{v}_{s,k} = [\tilde{v}_{sd,k} \ \tilde{v}_{sq,k}]^\top$ is the ideal (commanded) stator voltage vector, $\tilde{i}_{s,k} = [i_{sd,k} \ i_{sq,k}]^\top$ is the measured stator current vector, t_d is the dead-time, f_{sw} is the switching frequency of the power electronics (in Hertz) and V_{bus} is the DC bus voltage. The sinusoidal first-harmonic of the square-wave dead-time voltage is used to avoid introducing the additional harmonic content associated with the *sign* function.

Finally, we note that the exponential term in (29) is used to compensate for the time delay present in the experimental sampled-data implementation. While a stator current predictor could be employed to compensate the time delay, it would require accurate knowledge of the machine parameters (which we are trying to identify). Instead, we simply advance the normalized stator current vector by 1.5 times the angular distance traveled by the stator current vector over one sample period. The factor of 1.5 is used to center the prediction over the next sample period, which was found to provide improved performance in numerical simulations.

IV. STATOR FLUX LINKAGE ESTIMATION

Accurate estimation of the stator flux linkage is necessary for the proposed parameter identification technique, as well as for field-oriented control techniques in general. In particular, consideration must be given to the sampled-data nature of modern

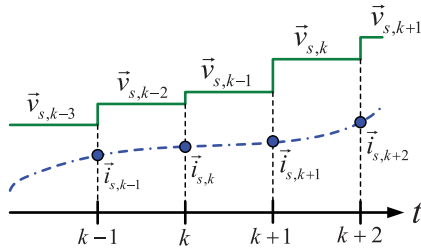


Fig. 6. Timing relationships for sampled-data implementation with unit delay.

controller implementations, which include a time delay between when stator currents are sampled and when the computed duty cycle is executed.

Typically, the stator flux linkage is estimated by integrating the stator flux linkage dynamics (1). In general, the stator flux linkage vector at time t_k is given by

$$\vec{\lambda}_{s,k} = \vec{\lambda}_{s,k-1} + \int_{t_{k-1}}^{t_k} (\vec{v}_s(t) - R_s \vec{i}_s(t)) dt. \quad (30)$$

We will assume that the voltage applied to the stator terminals is constant over a given sample period, T_s , which is true in an average-value sense, and that there is a one sample-period delay before a computed voltage is applied, as depicted in Fig. 6. In other words, the voltage/duty cycle computed at time index k is applied at $k+1$. Under these assumptions, the discrete-time estimate of the stator flux linkage at time k is given by

$$\hat{\vec{\lambda}}_{s,k} = \hat{\vec{\lambda}}_{s,k-1} + T_s \vec{e}_{s,k}, \quad (31)$$

with

$$\vec{e}_{s,k} = \tilde{\vec{v}}_{s,k-2} - \frac{R_s}{2} (\vec{i}_{s,k} + \vec{i}_{s,k-1}), \quad (32)$$

where $\tilde{\vec{v}}_{s,k-2}$ denotes the *commanded* voltage computed at time index $k-2$ (which is implemented at $k-1$), $\vec{i}_{s,k}$ and $\vec{i}_{s,k-1}$ denote the *measured* stator current at time index k and $k-1$, respectively. In the z -domain, (31) may be represented by the following transfer function

$$\hat{\vec{\lambda}}_{s,k} = \left\{ \frac{zT_s}{z-1} \right\} \vec{e}_{s,k}. \quad (33)$$

Note that $\vec{e}_{s,k}$ is essentially an input to the discrete-time integrator in (33). However, the use of a pure integrator is undesirable in practice, as it can lead to drift and instabilities. Instead, we use a discrete-time approximation of a stable second-order continuous-time integrator approximation.

To reject DC biases in the measured currents, and achieve a faster phase transition (to 90°) we employ a second-order integrator approximation [6],

$$\hat{\vec{\lambda}}_s = \left\{ \frac{s}{s^2 + 2\zeta\omega_n s + \omega_n^2} \right\} (\vec{v}_s - R_s \vec{i}_s), \quad (34)$$

where “ s ” is the Laplace variable, $\zeta > 0$ is the damping constant, ω_n sets the corner frequency of the integrator approximation, and the brackets, e.g., $\{F(s)\}$, are used to indicate a dynamic operator with transfer function $F(s)$. To ensure accurate estimates of the stator flux linkage, ω_n should be set as

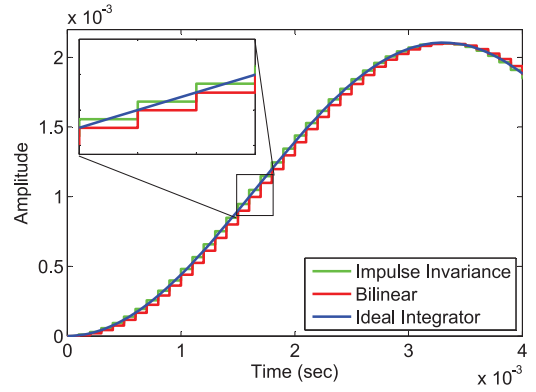


Fig. 7. Comparison of bilinear and impulse invariance discrete-time second order integrator approximations with ideal continuous-time integrator.

low as possible⁴ (i.e., $\omega_n \leq 0.01 \Omega_e$) while still providing stable flux linkage estimates. While the discussion of continuous-time representations is conceptually convenient, discrete-time implementations must be derived for experimental implementation on a microcontroller.

Two common methods for deriving discrete-time approximations of continuous-time transfer functions are the bilinear transform and the impulse invariance method [32]. While the bilinear transform is generally favored for filter design, it leads to a small delay in our application, which is avoided by using the impulse invariance method, as shown in Fig. 7. Using the impulse invariance method, the following discrete-time integrator approximation is obtained for $\zeta = 0.4$ and $\omega_n = 5$ rad/sec

$$\hat{\vec{\lambda}}_{s,k} = \left\{ \frac{0.0001z^2 - 0.0001z}{z^2 - 2z + 0.9999} \right\} \vec{e}_{s,k}, \quad (35)$$

where the coefficients are computed using MATLAB’s *c2d* command, which converts continuous-time system models to a discrete-time equivalent using the method specified (e.g., ‘*impulse*’ for the impulse invariance method).

V. NUMERICAL ANALYSIS

Numerical simulations implemented in MATLAB/Simulink are used to evaluate the proposed parameter identification methodology’s accuracy in the presence of non-ideal effects which are encountered in experimental implementations. Specifically, our simulations include non-ideal inverter characteristics such as dead-time, switch resistance, and diode voltage drops, as well as the sampled-data nature of experimental implementations, which include a one-time-step delay. Additionally, zero-mean Gaussian noise, of amplitude (i.e., variance) comparable to what we have observed in our experimental test-bed, is added to the three-phase stator current measurements.

To capture the sampled-data nature of the experimental system, our algorithm is implemented in a triggered subsystem in Simulink, while the machine dynamics are simulated in a continuous-time environment using MATLAB’s *ode45* solver. To reduce simulation times, an “average-value” inverter model is used. That is, we do not model the switching nature of the

⁴Note that $F(s) \approx \frac{1}{s}$ for $\omega \gg \omega_n$.

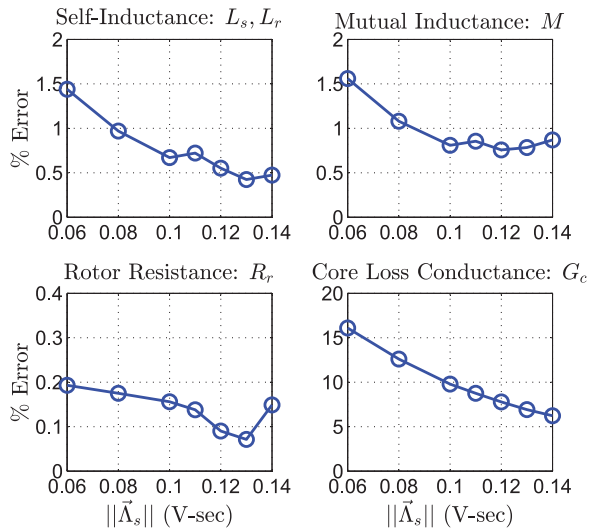


Fig. 8. Simulated parameter errors with non-ideal effects similar to experimental conditions.

inverter, since the switching frequency is high enough that its impact on performance is negligible. We do, however, model the dead-time effect and other non-ideal effects (resistive and diode voltage drops of the IGBT switches) by appropriately modifying the voltage commands produced by the identification algorithm before they are fed to the induction machine model.

The methodology for data collection and parameter identification control algorithm (Fig. 4) with stator flux linkage estimation, described in the prequel, were used to generate the numerical data from MATLAB/Simulink at various slip frequencies. The simulated data was generated at a variety of flux linkage magnitudes ranging from 0.06 V-sec to 0.14 V-sec, closely mimicking the experimental conditions (same bus voltage, sampling frequency, etc.) and using machine parameter values similar to those of the test machine. An electrical base frequency of 153.33 Hz was used, which corresponds to a zero-slip rotor speed of 4600 rpm (i.e., the rated rotor speed of the experimental test machine). The simulated data was then used to compute the machine parameters in the same fashion that the experimental data is processed, using the proposed technique discussed earlier. The resulting parameter errors are plotted in Fig. 8 as a function of flux linkage magnitude.

Inspection of the simulation results in Fig. 8 reveals that the proposed parameter identification methodology is capable of estimating the magnetic parameters and rotor resistance with high accuracy in the presence of non-ideal effects. Additionally, while the core loss conductance proves to be a more challenging parameter to estimate, the proposed technique provides estimates with reasonable and consistent accuracy, which improve at higher flux linkage magnitudes. This is due to the fact that the dead-time effect, as well as the transistor voltage drops, result in a fixed magnitude voltage error. And so, their impact on the accuracy of estimated parameter diminishes as voltage levels increase with higher flux linkage magnitudes, as well as higher speeds. It is also worth noting that, by including core loss in the model, the estimation of other parameters is improved.

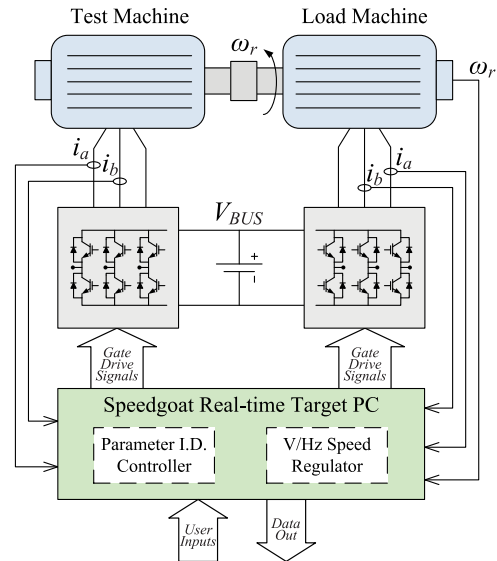


Fig. 9. Experimental setup for parameter identification data collection.

VI. EXPERIMENTAL RESULTS

A. Experimental Setup

The experimental parameter identification control algorithm is implemented on a Speedgoat real-time target machine using auto-generated code from MATLAB/Simulink. The test motor is a 3-phase, 4,600 rpm (nominal), 43 kW-peak induction machine from Azure Dynamics, driven by an IGBT inverter with a switching frequency of 10 kHz, bus voltage of 300 V, and dead-time of 2 μ s. A center-based pulse-width modulation is employed to synchronize sampling and switching, thereby avoiding the pickup of electromagnetic interference generated during switching transitions. Thus, the control algorithm for parameter identification is executed at 10 kHz as well, and Space-Vector Modulation (SVM) is used to generate the desired duty-cycles sent to the inverter. An identical induction machine serves as the load for the test machine by regulating the rotor speed (Fig. 9). Finally, a photograph of the experimental hardware is provided in Fig. 10.

B. Experimentally Identified Parameters

Steady-state data is recorded for several stator flux linkage magnitudes, ranging from 0.08 V-sec to 0.14 V-sec, at an electrical base frequency of 153.33 Hz. For each flux linkage magnitude, the direct and quadrature currents (in the stator flux linkage reference-frame) are recorded for several different slip frequencies, including zero-slip, roughly up to the current limitations of the machines. The resulting machine parameters, estimated using the proposed technique, are plotted in Fig. 11 as a function of stator flux linkage magnitude, $\|\vec{\lambda}_s\|$.

Inspection of the parameter estimates in Fig. 11 reveals that the estimated self and mutual inductance capture the saturation effects in the machine. As for the estimated rotor resistance, while there are some variations in the estimates, these variations are well within the range expected due to temperature

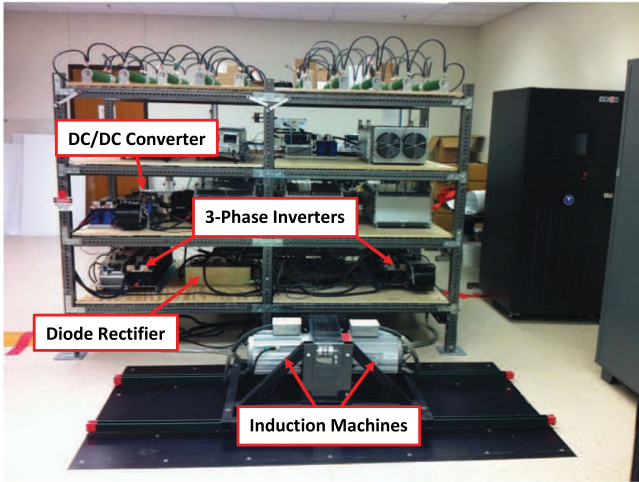


Fig. 10. Photograph of the experimental equipment (Not pictured: Speedgoat real-time controller and Zimmer power analyzer).

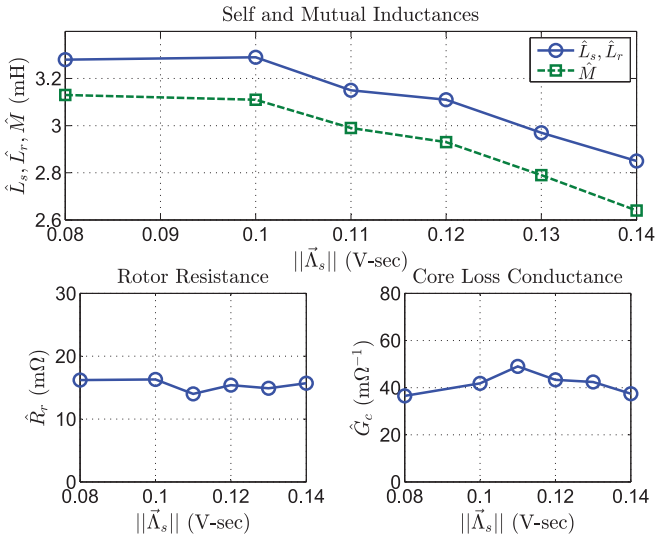


Fig. 11. Experimental estimated machine parameters as a function of stator flux linkage magnitude.

changes. In fact, the lower resistance estimate at 0.11 V-sec corresponds to data collected after allowing the machine time to cool down in between data collections. Finally, inspection of Fig. 11 reveals that the core loss conductance estimates are reasonably consistent across all of the stator flux linkage magnitudes. Finally, the experimental stator current locus plots for several stator flux linkage magnitudes are provided in Fig. 12. The estimated locus points are computed using the estimated machine parameters along with equations (11) and (12). Inspection of Fig. 12 reveals that there is a good consensus between the experimental (blue circles) and estimated (red X's) locus points.

C. Experimental Validation

To validate the proposed parameter estimation technique, the IEEE standard is used to provide alternative estimates of the induction machine parameters. It is then shown that model-based

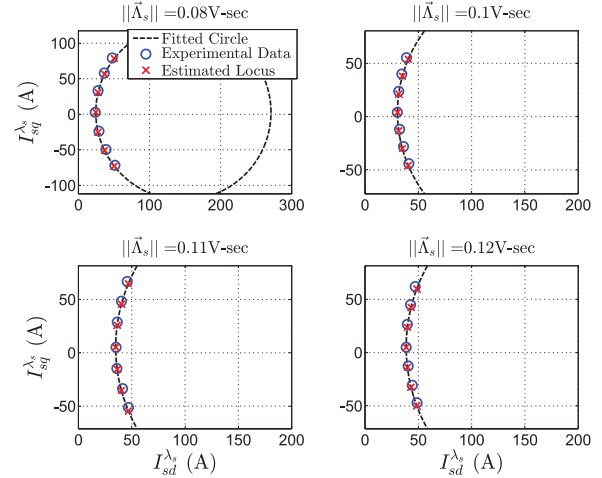


Fig. 12. Experimental data (blue circles) with fitted current locus circle (green dashed line) and estimated locus points (red X's) for various stator flux linkage magnitudes.

predictions of the steady-state machine behavior computed using the parameter estimates provided by the proposed technique are more accurate than those obtained using the IEEE standard when compared to measured values.

1) *IEEE Standard Parameters:* In order to conduct the IEEE standard tests for induction machine parameter identification [13], a single-stage three-phase LC-filter is constructed to remove switching harmonics from the VSI outputs. Components used in the filter are matched to ensure that the filtered three-phase voltages are well balanced, and sized to yield a cutoff frequency of approximately 950 Hz⁵ (a little over a decade below the switching frequency).

The induction machine under test is decoupled from the load machine during the IEEE standard data collection. The no-load test is performed at the rated frequency of 153.33 Hz and the applied voltages are varied to generate data at approximately the same stator flux linkage magnitudes as the data presented in the previous section (i.e., $\|\vec{\Lambda}_s\| = 0.08, 0.10, 0.11, 0.12, 0.13$ and 0.14 V-sec) according to the following relationship: $\|\vec{V}_s\| \approx |\Omega_e| \cdot \|\vec{\Lambda}_s\|$. At each voltage/flux level, the RMS line current and three-phase input power are measured using a Zimmer LMG670 Precision Power Analyzer. The rotor is then blocked for the locked-rotor test, and the excitation frequency is reduced to 25% of the rated value (i.e., 38.33 Hz, per the IEEE standard). Additionally, the line-to-line excitation voltage is reduced to 10.48 volts RMS in order to limit the line current during the blocked-rotor test. Again, the RMS line current and three-phase input power are measured. The resulting estimated machine parameters are plotted versus stator flux linkage magnitude in Fig. 13.

2) *Comparison of Results:* To validate the proposed parameter estimation technique, steady-state measurements of the average RMS line current, power factor, and three-phase input power are recorded for various slip-frequencies (i.e., the test machine is loaded during the data collection) using a Zimmer LMG670

⁵Taking into account the approximate loading due to the machine impedance.

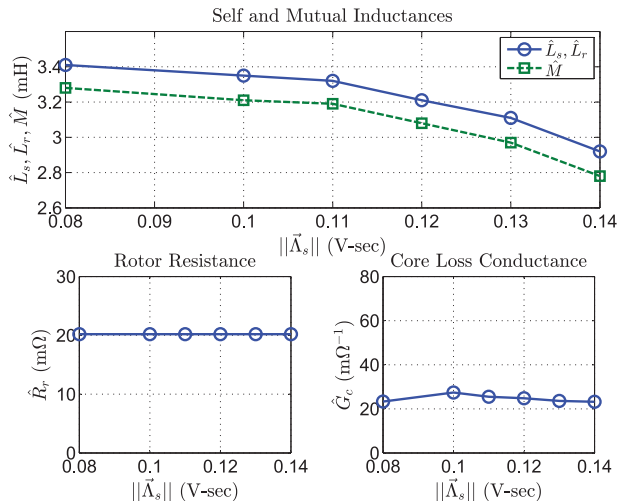


Fig. 13. IEEE standard estimated machine parameters as a function of stator flux linkage magnitude. Note that only a single value for rotor resistance, R_r , is obtained (it is plotted here simply for convenience).

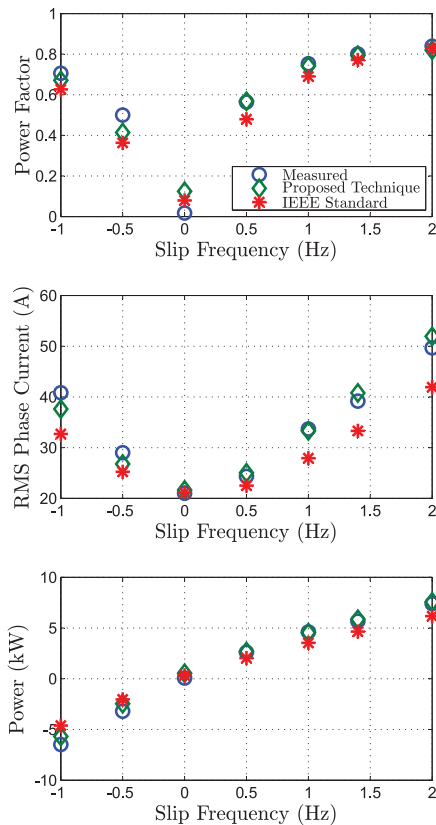


Fig. 14. Comparison of the predicted values to experimental measurements (blue circles) using parameters estimated using the proposed technique (green diamonds) and IEEE standard (red asterisks).

Precision Power Analyzer. The same experimental setup as in Fig. 9 is used, with the exception that inverter voltages feeding the Test Machine are low-pass filtered to remove harmonic content and conform to the IEEE standard limitation on total-harmonic distortion. Data is collected at the rated frequency of 153.33 Hz and at a voltage magnitude approximately corresponding to a stator flux-linkage magnitude of 0.1 V-sec. The

TABLE I
PARAMETERS USED IN MODEL-BASED PREDICTIONS

Description	Value
<i>Machine Parameters From Proposed Technique</i>	
Stator Resistance, R_s	22 m Ω
Self-Inductance, $L_{s,r}$	3.29 mH
Mutual Inductance, M	3.11 mH
Avg. Rotor Resistance, R_r	15.4 m Ω
Avg. Core Loss Conductance, G_c	41.7 m Ω^{-1}
<i>Machine Parameters From IEEE Standard</i>	
Stator Resistance, R_s	22 m Ω
Self-Inductance, $L_{s,r}$	3.35 mH
Mutual Inductance, M	3.21 mH
Avg. Rotor Resistance, R_r	20.2 m Ω
Avg. Core Loss Conductance, G_c	24.6 m Ω^{-1}

measurements are then compared to predictions based on the estimated parameters obtained using the proposed technique, as well as the IEEE standard for induction machine parameter estimation, and are provided in Fig. 14. The parameter values used to compute the predictions in Fig. 14 are provided in Table I and correspond to data obtained at a stator flux linkage magnitude of 0.1 V-sec, with the exceptions of rotor resistance and core loss conductance in which their average values were used. Inspection of these results reveals that the predictions based on parameters estimated using the proposed technique outperform those made using the IEEE standard, particularly under loaded (i.e., non-zero slip) conditions.

VII. CONCLUSION

This paper presented a new technique for offline identification of induction machine parameters, including core loss conductance, using steady-state measurements. The technique is based on fitting steady-state experimental data to the circular stator current locus in the stator flux linkage reference-frame for various steady-state slip frequencies, providing reliable estimates of the magnetic parameters as well as the rotor resistance and core loss conductance. This approach allows accurate estimation of leakage inductance and rotor resistance while avoiding the practical challenges of implementing a locked-rotor test with a voltage-source inverter. Numerical results verifying the accuracy of estimated parameters in the presence of non-ideal effects were presented, in addition to experimental results for a 43 kW induction machine, which demonstrate the proposed technique's ability to accurately characterize a VSI-driven induction machine over a wide range of operating conditions, including magnetic saturation. Finally, experimental results reveal that the predictions based on parameters estimated using the proposed technique outperform those made using the IEEE standard, particularly under loaded (i.e., non-zero slip) conditions.

ACKNOWLEDGMENT

The authors would like to thank A. Zeynu and J. Hou for their assistance with collecting the experimental data presented in this paper, and the reviewers for their valuable feedback which has undoubtedly improved this paper.

REFERENCES

- [1] R. Krishnan and F. C. Doran, "Study of parameter sensitivity in high-performance inverter-fed induction motor drive systems," *IEEE Trans. Ind. Appl.*, vol. IA-23, no. 4, pp. 623–635, Jul. 1987.
- [2] L.-C. Zai, C. DeMarco, and T. Lipo, "An extended Kalman filter approach to rotor time constant measurement in PWM induction motor drives," *IEEE Trans. Ind. Appl.*, vol. 28, no. 1, pp. 96–104, Jan. 1992.
- [3] H. Toliyat, E. Levi, and M. Raina, "A review of RFO induction motor parameter estimation techniques," *IEEE Trans. Energy Convers.*, vol. 18, no. 2, pp. 271–283, Jun. 2003.
- [4] C. Kwon and S. Sudhoff, "An on-line rotor resistance estimator for induction machine drives," in *Proc. 2005 IEEE Int. Conf. Elect. Mach. Drives*, May 2005, pp. 391–397.
- [5] R. Marino, S. Peresada, and P. Tomei, "On-line stator and rotor resistance estimation for induction motors," *IEEE Trans. Control Syst. Technol.*, vol. 8, no. 3, pp. 570–579, May 2000.
- [6] D. M. Reed and H. F. Hofmann, "Direct field-oriented control of an induction machine using an adaptive rotor resistance estimator," in *Proc. 2010 IEEE Energy Convers. Congr. Expo.*, Sep. 2010, pp. 1158–1165.
- [7] K. Wang, J. Chiasson, M. Bodson, and L. Tolbert, "An online rotor time constant estimator for the induction machine," *IEEE Trans. Control Syst. Technol.*, vol. 15, no. 2, pp. 339–348, Mar. 2007.
- [8] B. Bose, *Modern Power Electronics and AC Drives*. Englewood Cliffs, NJ, USA: Prentice-Hall, 2002.
- [9] M. Ranta and M. Hinkkanen, "Online identification of parameters defining the saturation characteristics of induction machines," *IEEE Trans. Ind. Appl.*, vol. 49, no. 5, pp. 2136–2145, Sep. 2013.
- [10] R. Lorenz, "A simplified approach to continuous on-line tuning of field-oriented induction machine drives," *IEEE Trans. Ind. Appl.*, vol. 26, no. 3, pp. 420–424, Mar. 1990.
- [11] J. Stephan, M. Bodson, and J. Chiasson, "Real-time estimation of the parameters and fluxes of induction motors," *IEEE Trans. Ind. Appl.*, vol. 30, no. 3, pp. 746–759, 1994.
- [12] J. Holtz and T. Thimm, "Identification of the machine parameters in a vector-controlled induction motor drive," *IEEE Trans. Ind. Appl.*, vol. 27, no. 6, pp. 1111–1118, Nov. 1991.
- [13] "IEEE standard test procedure for polyphase induction motors and generators," *IEEE Std 112-2004 (Revision of IEEE Std 112-1996)*, 2004.
- [14] K. Wang, J. Chiasson, M. Bodson, and L. Tolbert, "A nonlinear least-squares approach for identification of the induction motor parameters," *IEEE Trans. Automat. Control*, vol. 50, no. 10, pp. 1622–1628, Oct. 2005.
- [15] Y. He, Y. Wang, Y. Feng, and Z. Wang, "Parameter identification of an induction machine at standstill using the vector constructing method," *IEEE Trans. Power Electron.*, vol. 27, no. 2, pp. 905–915, Feb. 2012.
- [16] H. Kojooyan-Jafari, L. Monjo, F. Corcoles, and J. Pedra, "Parameter estimation of wound-rotor induction motors from transient measurements," *IEEE Trans. Energy Convers.*, vol. 29, no. 2, pp. 300–308, Jun. 2014.
- [17] W.-M. Lin, T.-J. Su, and R.-C. Wu, "Parameter identification of induction machine with a starting no-load low-voltage test," *IEEE Trans. Ind. Electron.*, vol. 59, no. 1, pp. 352–360, Jan. 2012.
- [18] J. Ruan and S. Wang, "A prediction error method-based self-commissioning scheme for parameter identification of induction motors in sensorless drives," *IEEE Trans. Energy Convers.*, vol. 30, no. 1, pp. 384–393, Mar. 2015.
- [19] S. Shaw and S. Leeb, "Identification of induction motor parameters from transient stator current measurements," *IEEE Trans. Ind. Electron.*, vol. 46, no. 1, pp. 139–149, Feb. 1999.
- [20] B. Abdelhadi, A. Benoudjit, and N. Nait-Said, "Application of genetic algorithm with a novel adaptive scheme for the identification of induction machine parameters," *IEEE Trans. Energy Convers.*, vol. 20, no. 2, pp. 284–291, Jun. 2005.
- [21] A. M. Alturas, S. M. Gadoue, B. Zahawi, and M. A. Elgendy, "On the identifiability of steady-state induction machine models using external measurements," *IEEE Trans. Energy Convers.*, vol. 31, no. 1, pp. 251–259, Mar. 2016.
- [22] Y.-S. Kwon, J.-H. Lee, S.-H. Moon, B.-K. Kwon, C.-H. Choi, and J.-K. Seok, "Standstill parameter identification of vector-controlled induction motors using the frequency characteristics of rotor bars," *IEEE Trans. Ind. Appl.*, vol. 45, no. 5, pp. 1610–1618, Sep. 2009.
- [23] L. Monjo, H. Kojooyan-Jafari, F. Corcoles, and J. Pedra, "Squirrel-cage induction motor parameter estimation using a variable frequency test," *IEEE Trans. Energy Convers.*, vol. 30, no. 2, pp. 550–557, Jun. 2015.
- [24] M. Al-Badri, P. Pillay, and P. Angers, "A novel algorithm for estimating refurbished three-phase induction motors efficiency using only no-load tests," *IEEE Trans. Energy Convers.*, vol. 30, no. 2, pp. 615–625, Jun. 2015.
- [25] M. Al-Badri, P. Pillay, and P. Angers, "A novel in situ efficiency estimation algorithm for three-phase IM using GA, IEEE method F1 calculations, and pretested motor data," *IEEE Trans. Energy Convers.*, vol. 30, no. 3, pp. 1092–1102, Sep. 2015.
- [26] S. Wade, M. Dunnigan, and B. Williams, "Improving the accuracy of the rotor resistance estimate for vector-controlled induction machines," *Elect. Power Appl. IEE Proc.*, vol. 144, no. 5, pp. 285–294, Sep. 1997.
- [27] D. Chatterjee, "Impact of core losses on parameter identification of three-phase induction machines," *IET Power Electron.*, vol. 7, no. 12, pp. 3126–3136, 2014.
- [28] D. M. Reed, K. Zhou, H. F. Hofmann, and J. Sun, "A stator current locus approach to induction machine parameter estimation," in *Proc. 2014 IEEE Conf. Expo Transp. Electrification Asia-Pacific*, Aug. 2014, pp. 1–6.
- [29] W. Duesterhoeft, M. W. Schulz, and E. Clarke, "Determination of instantaneous currents and voltages by means of alpha, beta, and zero components," *Trans. Amer. Inst. Electr. Eng.*, vol. 70, no. 2, pp. 1248–1255, Jul. 1951.
- [30] R. Park, "Two-reaction theory of synchronous machines, generalized method of analysis—Part 1," *A.I.E.E. Trans.*, vol. 48, pp. 81–95, 1929.
- [31] D. Umbach and K. Jones, "A few methods for fitting circles to data," *IEEE Trans. Instrum. Meas.*, vol. 52, no. 6, pp. 1881–1885, Dec. 2003.
- [32] J. G. Proakis and D. K. Manolakis, *Digital Signal Processing*, 4th ed. Upper Saddle River, NJ, USA: Prentice-Hall, 2006.



David M. Reed received the Bachelor's and Master's degrees in electrical engineering from the Pennsylvania State University (University Park), State College, PA, USA, and the Ph.D. degree in electrical engineering-systems from the University of Michigan, Ann Arbor, MI, USA, in 2007, 2009, and 2016, respectively. He is currently a Postdoctoral Research Fellow in the Department of Aerospace Engineering, University of Michigan. From 2009 to 2011, he was an Associate Staff Member in MIT Lincoln Laboratory, where he worked on a variety of projects ranging

from power supplies for satellite payloads, to controls for airborne optical sensor platforms. His current research focuses on the application of nonlinear, adaptive, and optimization-based control techniques to various problems in electric drives, energy systems, and engine control.



Heath F. Hofmann received the Ph.D. degree in electrical engineering and computer science from the University of California, Berkeley, CA, USA, in 1998. He is currently an Associate Professor with the University of Michigan, Ann Arbor, MI, USA. His research focuses on power electronics, specializing in the design, simulation, and control of electromechanical systems. His research interests include adaptive control techniques, energy harvesting, flywheel energy storage systems, electric and hybrid electric vehicles, and finite element analysis. He has published approx-

imately 40 papers in refereed journals, and has been awarded 13 patents.



Jing Sun received the Bachelor's and Master's degrees from the University of Science and Technology of China, Hefei, Anhui, China, and the Ph.D. degree from the University of Southern California, Los Angeles, CA, USA, in 1982, 1984, and 1989, respectively. She is the Michael G. Parsons Professor of Engineering at the University of Michigan, Ann Arbor, MI, USA. From 1989–1993, she was an Assistant Professor in the Electrical and Computer Engineering Department, Wayne State University. She joined the Ford Research Laboratory in 1993, where she worked

on advanced powertrain system controls. After spending almost 10 years in industry, she came back to academia in 2003 and joined the Naval Architecture and Marine Engineering Department, University of Michigan. She also has joint appointments in the Electrical Engineering and Computer Science Department as well as the Mechanical Engineering Department at the same university. She holds 39 US patents and has co-authored (with Petros Ioannou) a textbook on robust adaptive control. She has published more than 200 archived journal and conference papers. She received the 2003 IEEE Control System Technology Award.